Clinical and Translational Radiation Oncology 28 (2021) 62–70

Contents lists available at ScienceDirect

Clinical and Translational Radiation Oncology

journal homepage: www.elsevier.com/locate/ctro

Original Research Article

Ultrasound delta-radiomics during radiotherapy to predict recurrence in patients with head and neck squamous cell carcinoma

Kashuf Fatima [a], Archya Dasgupta [a,b,c], Daniel DiCenzo [a], Christopher Kolios [a], Karina Quiaoit [a], Murtuza Saifuddin [a], Michael Sandhu [a], Divya Bhardwaj [a], Irene Karam [b,c], Ian Poon [b,c], Zain Husain [b,c], Lakshmanan Sannachi [a], Gregory J. Czarnota [a,b,c,d,*]

[a] Physical Sciences, Sunnybrook Research Institute, Toronto, Canada
[b] Department of Radiation Oncology, Sunnybrook Health Sciences Centre, Toronto, Canada
[c] Department of Radiation Oncology, University of Toronto, Toronto, Canada
[d] Department of Medical Biophysics, University of Toronto, Toronto, Canada

ARTICLE INFO

Article history:
Received 23 December 2020
Revised 23 February 2021
Accepted 7 March 2021
Available online 12 March 2021

Keywords:
Radiomics
Delta-radiomics
Head and neck malignancy
Radiotherapy squamous cell carcinoma
Recurrence
Quantitative ultrasound
Machine learning

ABSTRACT

Purpose: This study investigated the use of quantitative ultrasound (QUS) obtained during radical radiotherapy (RT) as a radiomics biomarker for predicting recurrence in patients with node-positive head-neck squamous cell carcinoma (HNSCC).

Methods: Fifty-one patients with HNSCC were treated with RT (70 Gy/33 fractions) (±concurrent chemotherapy) were included. QUS Data acquisition involved scanning an index neck node with a clinical ultrasound device. Radiofrequency data were collected before starting RT, and after weeks 1, and 4. From this data, 31 spectral and related-texture features were determined for each time and delta (difference) features were computed. Patients were categorized into two groups based on clinical outcomes (recurrence or non-recurrence). Three machine learning classifiers were used for the development of a radiomics model. Features were selected using a forward sequential selection method and validated using leave-one-out cross-validation.

Results: The median follow up for the entire group was 38 months (range 7–64 months). The disease sites involved neck masses in patients with oropharynx (39), larynx (5), carcinoma unknown primary (5), and hypopharynx carcinoma (2). Concurrent chemotherapy and cetuximab were used in 41 and 1 patient(s), respectively. Recurrence was seen in 17 patients. At week 1 of RT, the support vector machine classifier resulted in the best performance, with accuracy and area under the curve (AUC) of 80% and 0.75, respectively. The accuracy and AUC improved to 82% and 0.81, respectively, at week 4 of treatment.

Conclusion: QUS Delta-radiomics can predict higher risk of recurrence with reasonable accuracy in HNSCC.

Clinical trial registration: clinicaltrials.gov.in identifier NCT03908684.

1. Introduction

Head and neck (HN) cancers are the seventh most common malignancy globally in 2018[1], with the majority arising from the epithelial lining representing squamous cell histology [2,3]. Head and neck squamous cell carcinoma (HNSCC) originating from the oropharynx, hypopharynx, and larynx are primarily treated with radical radiotherapy (RT), with or without concurrent

Abbreviations: QUS, Quantitative ultrasound; HNSCC, Head and neck squamous cell carcinoma; RT, Radiotherapy; CR, Complete responders; PR, Partial responders; RFS, Recurrence-free survival; R, Recurrence; NR, Non-recurrence; HN, Head and neck; HPV, Human papillomavirus; EBV, Epstein-Barr virus; IMRT, Intensity-modulated radiation therapy; IGRT, Image-guided radiation therapy; MRI, Magnetic resonance imaging; CT, Computed tomography; PET, Positron emission tomography; US, Ultrasound; RF, Radiofrequency; ROI, Region of interest; SS, Spectral slope; SI, Spectral intercept; MBF, Mid-band fit; AAC, Average acoustic concentration; ASD, Average scatterer diameter; ACE, Attenuation co-efficient estimate; SAS, Spacing among scatterers; GLCM, Grey level co-occurrence matrix; ENE, Energy; CON, Contrast; HOM, Homogeneity; COR, Correlation; FLD, Fisher's linear discriminant; *k*NN, *k* nearest neighbors; SVM, Support vector machine; TP, True positive; TN, True negative; FP, False positive; FN, False negative; S_n, Sensitivity; S_P, Specificity; Acc, Accuracy; AUC, Area under the curve; FDG-PET, ^{18}F-fluorodeoxyglucose positron emission tomography.

* Corresponding author at: Sunnybrook Health Sciences Centre, 2075 Bayview Avenue, T2, Toronto, Ontario M4N3M5, Canada.
E-mail address: gregory.czarnota@sunnybrook.ca (G.J. Czarnota).

https://doi.org/10.1016/j.ctro.2021.03.002

chemotherapy, decided by disease stage and patient-related factors [3]. Given the variable outcomes across individuals with HNSCC, it is prudent to develop suitable prognostic and predictive markers to facilitate the adoption of differential treatment strategies, finding an optimal balance between cure and toxicity [4,5]. 'Radiomics' is an emerging field in medicine where computational techniques are used to extract information from images that can reflect underlying tumor biology [6,7]. The potential of using images as non-invasive biomarkers has generated a surging interest in the oncology community to guide the way towards personalized medicine [8]. Radiomic analysis can be undertaken on standard imaging modalities like magnetic resonance imaging (MRI), computed tomography (CT), positron emission tomography (PET), and ultrasound (US), which are used in clinical management for patients with HNSCC. A common application of HN radiomics has been used to link imaging features with molecular characteristics, clinical outcomes like local recurrence, distant metastasis, overall survival, and others [9–11].

Conventional or bright mode (B-mode) US imaging presents a morphological representation of tissue obtained from underlying radiofrequency (RF) data converted into images. However, in this process, the frequency-dependent information from tissue structure is lost. The critical premise of quantitative ultrasound (QUS) is the processing of raw RF data from tissue backscatters, which can be used to characterize and distinguish phenotypic changes within a region of interest at a cellular level [12]. In preclinical studies, QUS had demonstrated efficacy in detecting treatment effects of various forms of cancer therapies [13–17]. QUS is sensitive to cell death-related structural changes even within 24 h, or clinically week 1 of treatment, arising from the changes in ultrasound scatterer elastic properties with phenomena like nuclear condensation, fragmentation, and the formation of apoptotic bodies.

In previous studies, QUS-based radiomics have been shown to effectively predict the response to radical RT in patients with HNSCC [18,19]. In a recent study, we have demonstrated the use of QUS-radiomics in predicting the recurrence for HNSCC using pretreatment features [20]. QUS data was obtained from the metastatic lymph node in 51 patients with HNSCC. A *k* nearest neighbors (*k*NN)-based model was able to predict patients developing recurrent disease with an accuracy of 75%, using the baseline imaging features alone. The current study was expanded to investigate the role of QUS parameters obtained during RT to detect the ongoing treatment-related changes at the cellular level and their influence on biological outcomes. This is the first study to use QUS delta-radiomics during radical RT in predicting recurrence.

2. Methods

2.1. Patients selection and treatment protocols

This prospective study was approved by the research ethics board at Sunnybrook Health Sciences Centre, Toronto, Canada, and Health Canada (clinicaltrials.gov identifier NCT03908684). Patients considered eligible for this study were required to have a metastatic lymph node (LN) amenable to US imaging. Metastatic involvement of LN was considered based on a combination of standard radiological features as reported, like increased size, rounded appearance, loss of fatty hilum, central necrosis, extracapsular extension, high metabolic activity (PET), or histological confirmation. Patients with histopathologically confirmed squamous cell carcinoma involving oropharynx, hypopharynx, larynx, and carcinoma unknown primary (CUP) were included. Primary disease from the oral cavity, nasopharynx, or CUP with the suspicion of nasopharyngeal primary were excluded. Written informed consent was obtained for all the patients. The study was conducted following good clinical practice and under the declarations of Helsinki.

All patients received radical RT using intensity modulated radiotherapy (IMRT) and image-guided techniques as per institutional practice, with 70 Gy/33 fractions in 6–7 weeks delivered to the high-risk volume (primary and nodes). Concurrent chemotherapy (cisplatinum) or other systemic therapy (cetuximab) was at the discretion of the medical oncologist. Recurrence was considered the endpoint for this study, confirmed by a clinical and radiological examination (histological confirmation in ambiguous scenarios) as decided by the clinician. The current study's primary objective was to test the performance of a quantitative analysis QUS in predicting the clinical outcomes. The driving principle of ultrasound-radiomics is to exploit the differential structural composition reflected as differences in elastic properties, which can vary and dictate the biological behavior. In breast malignancies, we have demonstrated the utility of ultrasound-radiomics in predicting the treatment response irrespective of the molecular subgroups [21]. Therefore, in the current study, other clinical features were not considered in the radiomics model development, as we aimed to investigate the classification performance of the imaging features alone. Patients were classified into two groups: exhibiting recurrence (R) and non-recurrence (NR). Any site of disease relapse (local, nodal, distant) was considered "recurrence" for study purposes. Patients who developed a second primary involving the HN or other anatomic sites were excluded. In the present analysis, patients with a minimum follow up of 12 months were included who did not have any evidence of disease recurrence. The clinical details pertinent to this study were obtained from a prospectively maintained database and electronic medical records review as required.

2.2. Ultrasound data acquisition

Fifty-one patients were enrolled in this study. For 45 patients, ultrasound RF data were acquired using a Sonix-RP based ultrasound system (Elekta Ltd, Montreal, Canada) with a linear 4-D transducer (4DL14-5/39 Linear 4D, BK Ultrasound, Peabody, MA, USA) with a center frequency of 6.5 MHz, bandwidth of 3 to 8 MHz, a sampling rate of 40 MHz, and 2.5 cm focus depth. For the remaining 6 patients, US data were acquired using a Sonix RP clinical ultrasound system (Analogic Medical Corp., Vancouver, Canada) with a linear array transducer (L14-5/60) operating at an equivalent center frequency of 6.5 MHz, a bandwidth of 3 to 8 MHz, a 40 MHz sampling frequency, and 1.75 cm focus depth. Previous studies have demonstrated that the data obtained from different US systems did not affect further image processing following appropriate normalization and pre-processing [22]. Ultrasound scans of the largest or most prominent involved LN were conducted before beginning RT (pretreatment) and then at 1 week and 4 weeks after the start of RT by expert sonographers. The responsible radiation oncologist identified the index LN. In the case of multiple metastatic nodes, the largest LN was considered appropriate for QUS imaging.

2.3. Quantitative ultrasound spectroscopy

B-Mode images were reconstructed from the RF data, and the LN was manually contoured to denote a region of interest (ROI) for the corresponding 2-D image. Three to five ROIs were selected from each ultrasound image at regularly spaced intervals. Each ROI was divided into window blocks (2 mm × 2 mm) using a sliding window approach for analysis with a 92% overlap along the axial and lateral direction.

A fast Fourier transform was applied to the raw RF data in each ROI window block to compute the power spectrum. To remove system transfer effects, the power spectrum was normalized with a reference power spectrum acquired from a tissue-mimicking reference phantom using the same device settings [23,24]. A total of seven spectral parameters were calculated within each ROI window. These include spectral slope (SS), spectral intercept (SI) at 0 MHz, mid-band fit (MBF), average acoustic concentration (AAC), average scatterer diameter (ASD), attenuation coefficient estimate (ACE), and spacing among scatterers (SAS). The spectral parameters served as the first-order imaging features. The details of data normalization and processing have been described in previous publications [21,24].

2.4. Texture analysis

The spectral data extracted from each ROI window was used to construct color-coded parametric maps based on the quantitative values of 6 spectral parameters (except ACE). Texture features were extracted from each QUS parametric map using a grey level co-occurrence matrix (GLCM) method [25]. Sixteen symmetric GLCMs were constructed from each parametric map, using pixel-neighbor distances of 1, 2, 3, and 4 pixels, and angles of 0°, 45°, 90°, and 135°. From each GLCM, four texture features, including energy (ENE), contrast (CON), homogeneity (HOM), and correlation (COR), were calculated and averaged [25].

In total, for each time point, 7 QUS parameters and 24 texture parameters were acquired from the RF data. The weighted average of the parameter obtained from all the ROIs was used as the feature metric. The differences between the values at week 1 and week 4 and the pretreatment values were used for model generation, labeled as delta-features. A combination set of baselines and delta features (baseline + delta-week1, baseline + delta-week4) was used for machine learning models. Therefore, a total set of 62 features was used at both time points.

2.5. Statistical tests

The distribution of the various clinical features (categorical data) between the two groups was compared using the Pearson chi-square test and Fisher's exact test. The mean and standard error of the mean were calculated for each QUS spectral and texture parameter for R and NR patients. To test the distribution of features, a Shapiro–Wilk test was done. To determine the distribution between the two groups, a *t*-test or Mann-Whitney *U* test was performed for normally distributed data and non-parametric data, respectively. A p-value of less than 0.05 was considered to be statistically significant.

2.6. Machine learning classification

Machine learning algorithms were used to classify the two outcome groups (R vs. NR) based on their QUS spectral and texture features. Three classification algorithms were used, including Fisher's linear discriminant (FLD), *k* nearest neighbors (*k*NN), and support vector machine (SVM). The models were tuned to select the best classifying feature using forward feature selection. To mitigate the curse of dimensionality and overfitting, a maximum of 3 features were used in the model. The models were trained using all 51 patients and tested using leave-one-out cross-validation. Since the two groups (R and NR) were not equally represented, subsets (n = 7) were generated by randomly selecting an equal number of patients from both the groups, without replacement. These subsets were then used as training data sets for the classifiers. The true-positive, true-negative, false-positive, and false-negative were calculated from the classifiers, which resulted in the indices-sensitivity (S_n), specificity (S_p), and accuracy (Acc). Receiver operator characteristic (ROC) curves were constructed, and the area under the curve (AUC) was computed.

The classification models assigned a recurrence label (predicted-R or predicted-NR) for each patient, which was used to calculate the predicted recurrence-free survival (RFS). The Kaplan Meier product-limit method was used for survival analysis (for calculation of RFS and overall survival), and the groups were compared using a log-rank test. The date of RT starting was considered as the baseline for survival analysis.

Tumor segmentation, extraction of imaging features from raw RF data, texture analysis, and machine learning classifications were done using MATLAB (2016a, MathWorks Inc., Natick, Massachusetts, United States).

3. Results

3.1. Patient and treatment characteristics

The median age was 59 years (range 40–70 years) for patients with recurrence, and 61 years (range 39–80 years) for patients with non-recurrence. Details of clinical and treatment characteristics are presented in Table 1. The most common primary site was the oropharynx with 39 patients, followed by larynx (5), carcinoma unknown primary (5), and hypopharynx (2). Forty-one patients received concurrent chemotherapy, 35 patients were administered cisplatin, 3 patients were administered carboplatin, and 1 had received cetuximab. Three patients who started with cisplatin dose were later switched to carboplatin. Nine patients were treated with definitive radiation alone.

3.2. Clinical outcomes

In patients without any disease recurrence, the median follow up was 42 months (range 14–59 months). In the entire cohort, the median follow up was 38 months (range 7–64 months), since patients with recurrent disease were included irrespective of follow up duration (including those with follow up < 12 months). Fifteen patients had a complete response to treatment, and 36 patients had a partial response to therapy at 3 months following completion of RT. Seventeen patients had recurrences, with the site of disease involvement during relapse as follows-isolated local (1), isolated nodal (2), local-nodal (1), isolated distant (8), nodal-distant (3), local-nodal-distant (2). The 2 and 5-year RFS were 72% and 62%, respectively. The median time to recurrence was 9 months (range 1–48 months), with 82% of recurrences occurring in the first 24 months. Overall survival (OS) for all patients was 90% and 64% at 2 years and 5 years, for R and NR patients, respectively.

3.3. Classification results and feature analysis

Ultrasound B-mode images and corresponding MBF, SI, AAC, ASD, SS, and SAS parametric maps of two representative patients, one from each of the outcome groups (R and NR), obtained at different times, are shown in Fig. 1. The parametric maps demonstrated evident intratumoral heterogeneity for the patients, as well as changes over time with treatment. One feature at week 1, ΔASD-ENE ($p = 0.041$), and four features at week 4, ΔMBF-ENE ($p = 0.027$), ΔMBF-HOM ($p = 0.032$), ΔSS-COR ($p = 0.049$), and ΔSI-HOM ($p = 0.020$) were found to be statistically different between R and NR, as noted in Supplementary Table 1 and the scatter plots shown in Fig. 2. The scatter plots for all QUS mean-value and textural parameters for R and NR at week 1 and week 4 are shown in Supplementary Figs. 1 and 2, respectively.

Table 1
Patient, disease, and treatment-related characteristics for all patients.

Clinical Characteristics		Recurrence (n=17)		n = 51 (All Subjects) Non-Recurrence (n = 34)	
Patient Characteristics		n	%	n	%
Age	Median	59 years		61 years	
	Range	40–70 years		39–80 years	
Gender	Female	0	0%	3	9%
	Male	17	100%	31	91%
Smoking Status	Smoker	12	71%	23	68%
	Non-Smoker	5	29%	11	32%
Disease Characteristics		n	%	n	%
T-stage	T0[a]	4	24%	1	3%
	T1	0	0%	14	41%
	T2	4	24%	14	41%
	T3	3	18%	2	6%
	T4	6	34%	3	9%
N-stage	N1	1	6%	21	62%
	N2	8	47%	12	35%
	N3	8	47%	1	3%
Tumor Grade	I	1	6%	0	0%
	II	1	6%	4	12%
	III	6	35%	12	35%
	Unclassified	9	53%	18	53%
Site	Oropharynx	10	59%	29	85%
	Hypopharynx	1	6%	1	3%
	Larynx	2	12%	3	9%
	CUP	4	24%	1	3%
HPV Status	p16(+)	8	47%	28	82%
	p16(−)	2	12%	0	0%
	Indeterminate/Unknown	7	41%	6	18%
Treatment Characteristics		n	%	n	%
Radiation + Chemotherapy (Concomitant)	Cisplatin	10	59%	25	74%
	Cisplatin → Carboplatin	1	6%	2	6%
	Carboplatin	1	6%	2	6%
Radiation + Targeted Therapy (Concomitant)	Cetuximab	1	6%	0	0%
Definitive Radiation Alone	Radiation Only	4	24%	5	15%

HPV: Human Papilloma Virus; CUP: Carcinoma of unknown primary origin.
[a] T0 denotes carcinoma of unknown primary.

The classification results obtained using FLD, *k*NN, and SVM algorithms are presented in Table 2. When comparing all classifiers, *k*NN and SVM performed better than FLD in predicting the recurrence group at all time points. The classifier indices continued to improve with the inclusion of delta-radiomic features during treatment, with the best results obtained during week 4. The SVM week 1 model demonstrated the classification performance of S_n 79%, S_p 80%, AUC 0.75, and Acc 80%. The model selected two features as ACE_0, ΔAAC-CON (the third feature was not chosen as there was no further improvement using a forward feature selection method with inclusion of the third feature). SVM Week 4 features, ACE_0, ΔSI-HOM, ΔSS-HOM, had an S_n 82%, S_p 82%, AUC 0.81, and Acc 82%. For the SVM model, the Acc and AUC using pretreatment features were 73% and 0.71, respectively. The Acc and AUC incorporating delta-week 1 features were 80% and 0.75, which further improved to 82% and 0.81 with delta-week 4 features, respectively. Fig. 3 represents the ROC curves of the three classifiers, FLD, *k*NN, and SVM, at pretreatment, week 1, week 4, clearly demonstrating the improvement of the AUC values with the week 1 and 4 delta-radiomic features.

Finally, each patient was assigned a specific group (predicted-R or predicted-NR) as determined by the classifiers. Fig. 4 represents SVM model-based group predictions at week 1 and the resulting impact on RFS and OS. Using the SVM-based model (both weeks 1 and 4), the predicted 3-year RFS was 90% and 32% for predicted-R and predicted-NR, respectively (p = <0.001) (Supplementary Table 2).

4. Discussion

Radiomics is an emerging field in medicine, with the potential to identify non-invasive biomarkers that can be used to tailor therapy on an individual basis, paving the way towards precision oncology [8]. Most of the studies in HN malignancies have used imaging modalities like CT, MRI, or PET, with limited literature related to US. In this study, QUS radiomic features during ongoing RT were investigated in terms of their capability to be used to predict recurrence for patients with HNSCC.

Computed tomography is commonly used in HNSCC cancer as a part of clinical management (diagnosis, staging, RT planning), and a multitude of studies have used CT radiomics for prognostication [26]. Leger *et al.* compared CT-derived radiomic features from baseline and week 2 scans for predicting locoregional tumor control in patients with HNSCC. It was found that the models trained using features from week 1 scans demonstrated am improved performance (C-Index 0.79) over the models trained using baseline scans (C-Index 0.65) [27]. Robin *et al.* used FDG PET-CT to detect recurrence for HNSCC patients 6 months after receiving RT, obtaining an overall accuracy of 89%, which is more accurate than physical examination alone [28]. Recently, more advanced classification algorithms have been implemented to determine significant texture features and their relationships automatically. Diamant *et al.* trained a convolutional neural network to predict distant metastasis with the CT data of 194 HNSCC patients, resulting in an AUC of 0.92 when combined with traditional radiomic models [29].

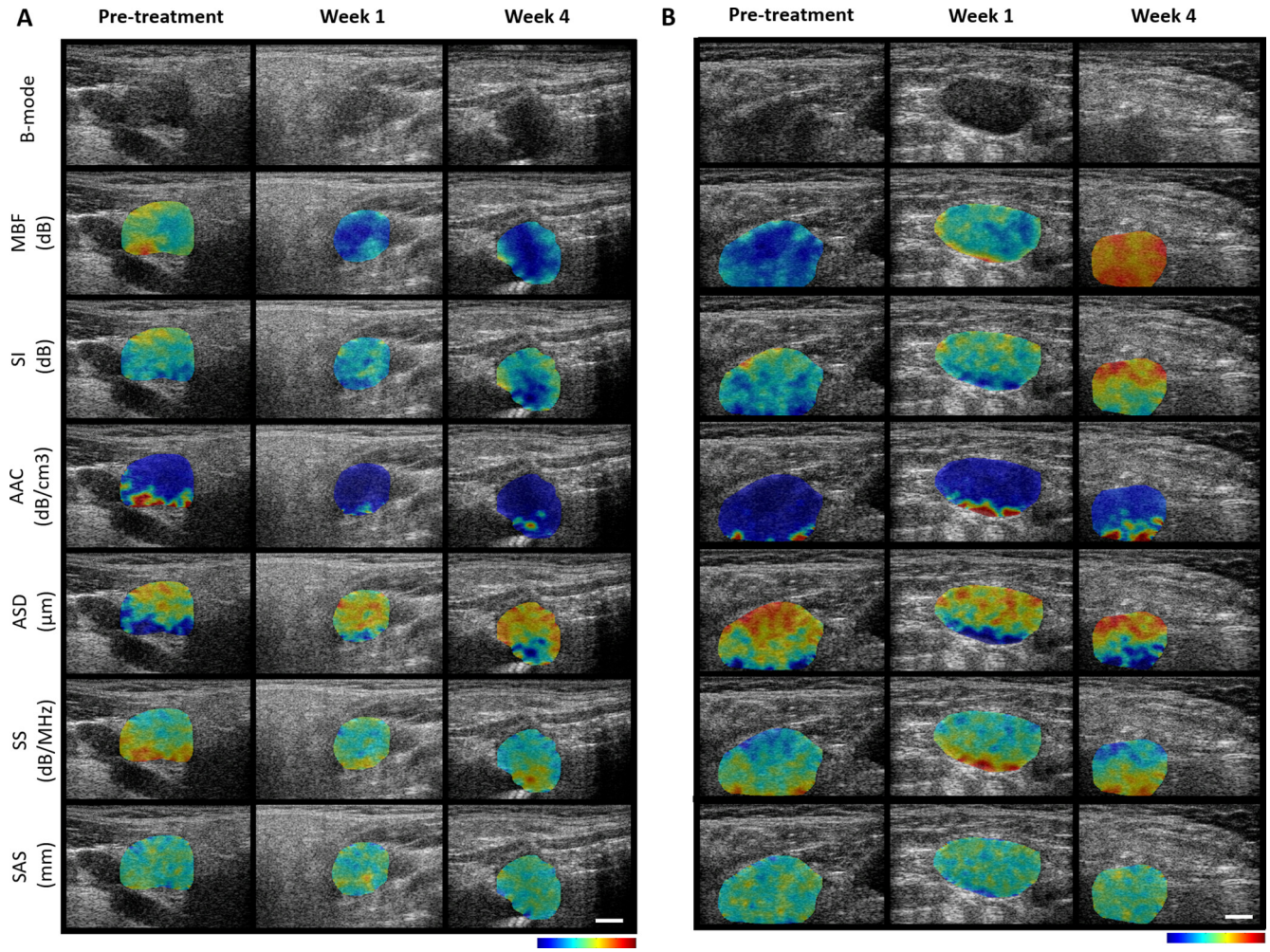

Fig. 1. Representative ultrasound B-mode images (upper row) with six representative texture-based parameters that have been acquired from one patient in each group – with recurrence (A) and without any recurrence (B) at different times: pretreatment, week 1, and week 4. Change in parameter values with treatment can be noted as represented by changes in assigned color to the sub-regions of interest within the tumor. The color-coded maps illustrate the intratumoral heterogeneity. With ongoing RT, individual QUS parameter changes can be visually appreciated, as evident from the associated color changes, reflecting treatment-related changes. The two patients (recurrence versus non-recurrence) show different patterns of changes. The white scale bar in ultrasound images represents 5 mm. The color bars present the range for MBF parameter of −10 dB to 24 dB, SI parameter of −8 dB to 60 dB, AAC parameter of 20 dB/cm-MHz to 170 dB/cm-MHz, ASD parameter of 1 μm to 200 μm, SS parameter of −7.97 dB/MHz to 2.63 dB/MHz, and SAS parameter of 0.15 mm to 2.50 mm.

Ultrasonography is more accessible than CT and MR and can be readily deployed easily in outpatient settings. QUS has been demonstrated to be an effective modality to predict treatment response in patients with breast cancer before starting chemotherapy [15]. Also, with the inclusion of features during treatment, the classification performances improved, consistent with the ability of QUS to pick up ongoing cellular changes with treatment [15]. Recently, Tran *et al.* used QUS-based radiomics to predict the response to RT patients with HNSCC cancer [19]. Whereas QUS was determined to be effective in response prediction, using recurrence as a clinical endpoint is beneficial as recurrence will ultimately have a more significant influence on final survival.

In the study, the best classifier was obtained using the SVM model (SVM-week 4: Acc = 82%, AUC = 0.81), the ΔSI-HOM, ΔSS-HOM, and ACE_0 were used. The baseline ACE represents tissue composition. The ΔSI-HOM represents the change in the homogeneity of pixel intensity levels in the SI parametric image, which is associated with the cells' acoustic properties (linked to scatterer concentration). The ΔSS-HOM represents the change in the homogeneity of the pixel intensity levels in the SS parametric image, which is associated with the size of the scatterers. It is known that tumor cells that respond to treatment undergo significant structural changes that modify ultrasound backscatter. Treatment-related changes in the tumor cells lead to changes in the tissue microstructure, leading to changes in the textual features reflected by temporal changes in high-output features or delta radiomics.

The models trained with the features that represented the change in QUS parameters from baseline to weeks 1 and 4 demonstrated better prediction performance than the models from the baseline data alone. This result is consistent with the observations made by Leger *et al.*, whose CT-derived HNSCC RT response prediction models showed increased accuracies with the inclusion of week 2 features [27]. It is common to find that the addition of intra-treatment texture features can improve the performance of texture-feature-derived radiomic models compared to pretreatment alone [21,27]. Jansen *et al.* found that some DCE MRI-derived imaging biomarkers for patients receiving chemoradiation treatment for HNSCC were significantly higher in intra-treatment scans versus pretreatment scans ($p < 0.04$) [30]. Our study indicates the efficiency of QUS-radiomics to detect RT-induced changes as early as into the first week of treatment and positively predicts the biological outcomes.

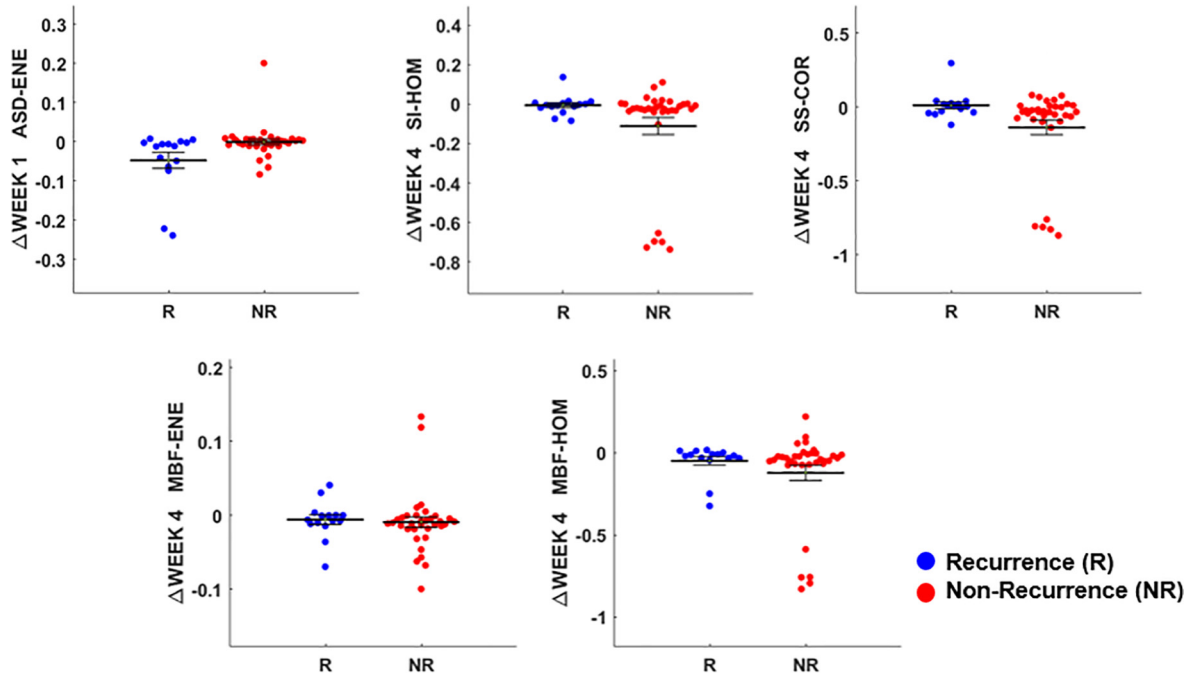

Fig. 2. Scatter plot showing the individual value from each patient for five parameters having a significant difference in distribution between the two groups (recurrence and non-recurrence).

Table 2
Classification performance of the three machine learning classifiers with the best-selected features by the algorithms obtained from different time points.

Model	Classification Performance	Sensitivity %	Specificity %	Accuracy %	AUC	Best Feature(s)		
FLD	Week 1	66	54	62	0.61	ΔASD-ENE	ΔAAC-CON	
	Week 4	64	67	65	0.68	ΔMBF-ENE	ΔSS-CON	ΔSAS
*k*NN	Week 1	85	65	78	0.75	$SS\text{-}ENE_0$	ΔSI	$SS\text{-}HOM_0$
	Week 4	82	82	82	0.83	SI_0	ΔSS-CON	ACE_0
SVM	Week 1	79	80	80	0.75	ACE_0	ΔAAC-CON	
	Week 4	82	82	82	0.81	ACE_0	ΔSI-HOM	ΔSS-HOM

AUC – Area under curve, FLD – Fisher's Linear Discriminate, *k*NN – *k* nearest-neighbors, SVM – Support vector machine.
*Δ Indicates the difference of values from baseline for each feature were included in the analysis.
MBF (dB): Mid-band fit, **AAC** (dB/cm^3): Average Acoustic Concentration, **ASD (μm):** Average Scatterer Diameter, **SS** (dB/MHz): Spectral Scope, **SAS (mm):** Spacing Among Scatterer, **ACE** (dB/cm-MHz): Attenuation Coefficient Estimate, **SI:** Spectral Intercept, **ENE:** Energy, **HOM:** Homogeneity, **COR:** Correlation, **CON:** Contrast.

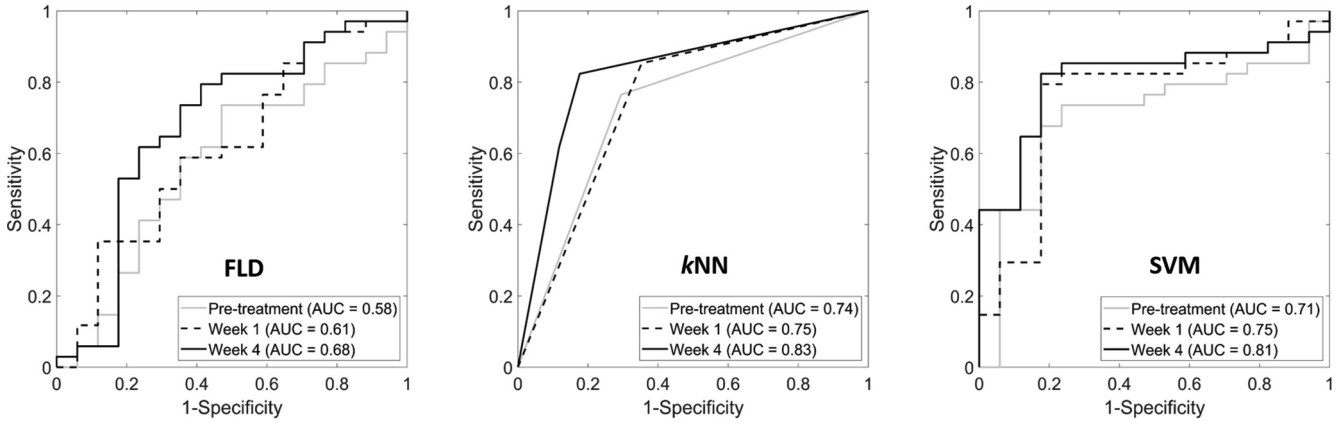

Fig. 3. Receiver operating characteristic (ROC) plots showing the area under the curve (AUC) values obtained from the three classifiers, FLD, *k*NN, and SVM, at week 0 (pretreatment), week 1, and week 4. FLD: Fisher's Linear Discriminant; *k*NN: *k* Nearest Neighbours; SVM: Support Vector Machine.

In this study, as we have included more features from the subsequent time points (week 1 and 4 of treatment), a higher number of features (double compared to baseline alone) are available for building the classifier models. An SVM model is known to work and classify better when a larger number of dimensions are present in the data. Therefore, the SVM-based model had better results in

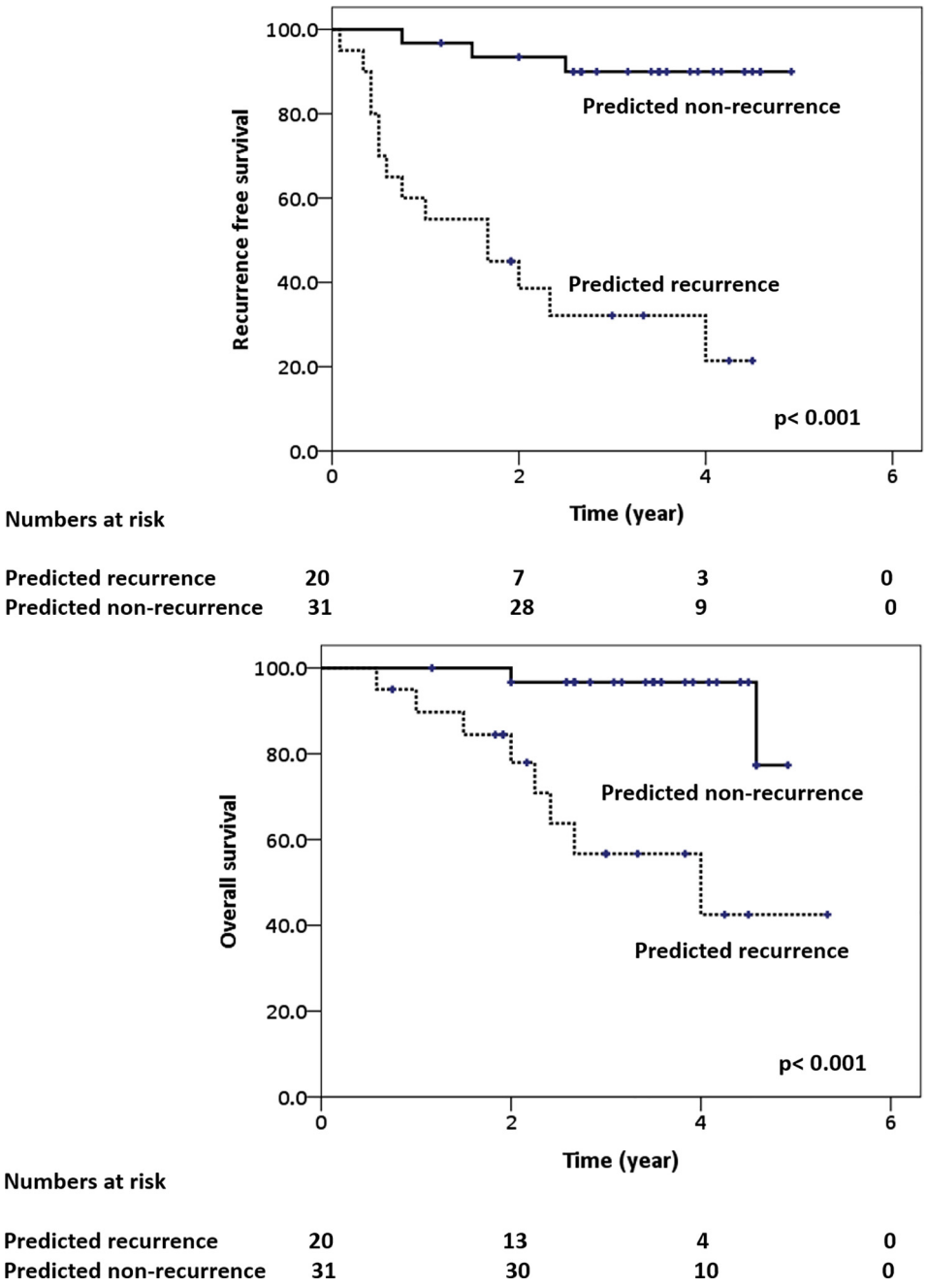

Fig. 4. Kaplan-Meier survival plots showing recurrence-free survival (A) and overall survival (B) based on predicted groups-recurrence (R) versus non-recurrence (NR)) using the support vector machine classifier at week 1.

the current study than the *k*NN in the previous study using pre-treatment features alone [20]. Also, in a smaller sample size like the present study, individual classifier performances' stability should be interpreted with caution, which will be minimized as more patients are included.

Radiomics has the potential to serve as a potent non-invasive biomarker in the assessment of early treatment response, providing opportunities for personalized radiotherapy. The traditional morphological and functional imaging-based response assessment is undertaken at approximately 12 weeks following treatment completion, leading to loss of window for early intervention for treatment-resistant disease. Using tools like QUS during treatment can enable early detection of treatment response and predict the clinical outcomes when such interventions can be undertaken in the form of dose-escalation or early referral for surgical intervention. Similarly, de-escalation strategies can be adopted in patients with good responses, leading to lesser probabilities of toxicities. At present adaptive strategies are not commonly used clinically as tools to facilitate them have not yet been developed generally or are limited. The approach here is an example of such a technology that will permit physicians to contemplate what therapy changes are best. For instance, "should radiotherapy be stopped at week 1 or week 4 and a surgeon asked to operate the patient instead of pursuing radiotherapy? Or should treatment continue to the planned end and refer the patient sooner for salvage?"

Being a pilot study, we had a limited number of patients in this analysis. With encouraging results, the current work is being expanded to include more patients. More patients will permit the

development of a more generalized prediction model, and appropriate internal validation strategies can be employed. In the future, we intend to undertake multi-institutional studies involving HNSCC, which will serve as an appropriate platform for undertaking external validation, to establish the clinical utility. It is recognized that the structure of metastatic nodes in p16+ patients is different (at least on CT/MRI) because of the pseudo-necrotic feature. Here we do not think this a confounding factor in this study as we suspect all nodes (p16 positive versus negative) were of significant size and exhibit some level of necrosis which likely plays a role in the analysis using texture-based features. With the inclusion of more patients, we will perform exploratory analysis to study the influence of various clinical features, as well as separate analyses for HPV-positive versus HPV-negative tumors. Also, with a higher number of patients, a combined clinical-radiomics model can be developed, which was not tested. The primary objective here was to investigate the utility of QUS-radiomics in detecting microstructural changes with treatment.

5. Conclusion

Machine learning classifiers trained with QUS spectral and texture parameters were shown to predict recurrence for patients with HNSCC receiving RT with an accuracy of 82% at week 4 of treatment. The classifier performance persistently improved from pretreatment into week 1 and week 4 with the inclusion of delta-radiomic features suggesting the utility of QUS to detect treatment-related changes in real-time and the implication on the clinical outcomes.

Declaration of Competing Interest

Gregory Czarnota received funding from Terry Fox Foundation Program Project Grant from the Hecht Foundation (grant number 1083). None of the other authors have any other conflict of interest to declare.

Acknowledgments

We would like to thank all of the patients who participated in the study. We would also like to express our sincere gratitude to the medical oncologists, radiation oncologists, and other healthcare professionals involved in patient care. The work was funded by Terry Fox Foundation Program Project Grant from the Hecht Foundation.

Funding

Terry Fox Foundation Program Project Grant from the Hecht Foundation (grant number 1083). The funding agency did not influence study design, conducting the study, data acquisition, or submitting the manuscript.

Appendix A. Supplementary data

Supplementary data to this article can be found online at https://doi.org/10.1016/j.ctro.2021.03.002.

References

[1] Bray F, Ferlay J, Soerjomataram I, Siegel RL, Torre LA, Jemal A. Global cancer statistics 2018: GLOBOCAN estimates of incidence and mortality worldwide for 36 cancers in 185 countries. CA Cancer J Clin 2018;68(6):394–424. https://doi.org/10.3322/caac.21492.

[2] Marur S, Forastiere AA. Head and neck squamous cell carcinoma: update on epidemiology, diagnosis, and treatment. Mayo Clin Proc 2016;91(3):386–96. https://doi.org/10.1016/j.mayocp.2015.12.017.

[3] Longo DL, Chow LQM. Head and neck cancer. N Engl J Med 2020;382(1):60–72. https://doi.org/10.1056/NEJMra1715715.

[4] Parmar C, Leijenaar RTH, Grossmann P, Velazquez ER, Bussink J, Rietveld D, et al. Radiomic feature clusters and prognostic signatures specific for lung and head & neck cancer. Sci Rep 2015. https://doi.org/10.1038/srep11044.

[5] Castelli J, Simon A, Lafond C, Perichon N, Rigaud B, Chajon E, De Bari B, Ozsahin M, Bourhis J, de Crevoisier R. Adaptive radiotherapy for head and neck cancer. Acta Oncol 2018;57(10):1284–92. https://doi.org/10.1080/0284186X.2018.1505053.

[6] Lambin P, Leijenaar RTH, Deist TM, Peerlings J, de Jong EEC, van Timmeren J, Sanduleanu S, Larue RTHM, Even AJG, Jochems A, van Wijk Y, Woodruff H, van Soest J, Lustberg T, Roelofs E, van Elmpt W, Dekker A, Mottaghy FM, Wildberger JE, Walsh S. Radiomics: the bridge between medical imaging and personalized medicine. Nat Rev Clin Oncol 2017;14(12):749–62. https://doi.org/10.1038/nrclinonc.2017.141.

[7] Gillies RJ, Kinahan PE, Hricak H. Radiomics: images are more than pictures, they are data. Radiology 2016;278(2):563–77. https://doi.org/10.1148/radiol.2015151169.

[8] Aerts HJWL. The potential of radiomic-based phenotyping in precision medicine: a review. JAMA Oncol 2016;2(12):1636. https://doi.org/10.1001/jamaoncol.2016.2631.

[9] Wong AJ, Kanwar A, Mohamed AS, Fuller CD. Radiomics in head and neck cancer: from exploration to application. Transl Cancer Res 2016;5(4):371–82. https://doi.org/10.21037/tcr.2016.07.18.

[10] Giraud P, Giraud P, Gasnier A, El Ayachy R, Kreps S, Foy J-P, et al. Radiomics and machine learning for radiotherapy in head and neck cancers. Front Oncol 2019;9:1–13. https://doi.org/10.3389/fonc.2019.00174.

[11] Haider SP, Burtness B, Yarbrough WG, Payabvash S. Applications of radiomics in precision diagnosis, prognostication and treatment planning of head and neck squamous cell carcinomas. Cancers Head Neck 2020;5(1). https://doi.org/10.1186/s41199-020-00053-7.

[12] Oelze ML, Mamou J. Review of quantitative ultrasound: envelope statistics and backscatter coefficient imaging and contributions to diagnostic ultrasound. IEEE Trans Ultrason, Ferroelect, Freq Contr 2016;63(2):336–51. https://doi.org/10.1109/TUFFC.2015.2513958.

[13] Czarnota GJ, Karshafian R, Burns PN, Wong S, Al Mahrouki A, Lee JW, Caissie A, Tran W, Kim C, Furukawa M, Wong E, Giles A. Tumor radiation response enhancement by acoustical stimulation of the vasculature. Proc Natl Acad Sci USA 2012;109(30):E2033–41. https://doi.org/10.1073/pnas.1200053109.

[14] Vlad RM, Brand S, Giles A, Kolios MC, Czarnota GJ. Quantitative ultrasound characterization of responses to radiotherapy in cancer mouse models. Clin Cancer Res 2009;15(6):2067–75. https://doi.org/10.1158/1078-0432.CCR-08-1970.

[15] DiCenzo D, Quiaoit K, Fatima K, Bhardwaj D, Sannachi L, Gangeh M, Sadeghi-Naini A, Dasgupta A, Kolios MC, Trudeau M, Gandhi S, Eisen A, Wright F, Look Hong N, Sahgal A, Stanisz G, Brezden C, Dinniwell R, Tran WT, Yang W, Curpen B, Czarnota GJ. Quantitative ultrasound radiomics in predicting response to neoadjuvant chemotherapy in patients with locally advanced breast cancer: results from multi-institutional study. Cancer Med 2020;9(16):5798–806. https://doi.org/10.1002/cam4.3255.

[16] Quiaoit K, DiCenzo D, Fatima K, Bhardwaj D, Sannachi L, Gangeh M, et al. Quantitative ultrasound radiomics for therapy response monitoring in patients with locally advanced breast cancer: multi-institutional study results. PLoS One 2020;15:e0236182. https://doi.org/10.1371/journal.pone.0236182.

[17] Dasgupta A, Brade S, Sannachi L, Quiaoit K, Fatima K, DiCenzo D, Osapoetra LO, Saifuddin M, Trudeau M, Gandhi S, Eisen A, Wright F, Look-Hong N, Sadeghi-Naini A, Tran WT, Curpen B, Czarnota GJ. Quantitative ultrasound radiomics using texture derivatives in prediction of treatment response to neo-adjuvant chemotherapy for locally advanced breast cancer. Oncotarget 2020;11(42):3782–92. https://doi.org/10.18632/oncotarget.27742.

[18] Tran WT, Suraweera H, Quaioit K, Cardenas D, Leong KX, Karam I, Poon I, Jang D, Sannachi L, Gangeh M, Tabbarah S, Lagree A, Sadeghi-Naini A, Czarnota GJ. Predictive quantitative ultrasound radiomic markers associated with treatment response in head and neck cancer. Future Sci OA 2020;6(1). https://doi.org/10.2144/fsoa-2019-0048. FSO433.

[19] Tran WT, Suraweera H, Quiaoit K, DiCenzo D, Fatima K, Jang D, et al. Quantitative ultrasound delta-radiomics during radiotherapy for monitoring treatment responses in head and neck malignancies. Future Sci OA 2020;6. https://doi.org/10.2144/fsoa-2020-0073. FSO624.

[20] Dasgupta A, Fatima K, DiCenzo D, Bhardwaj D, Quiaoit K, Saifuddin M, et al. Quantitative ultrasound radiomics in predicting recurrence for patients with node-positive head-neck squamous cell carcinoma treated with radical radiotherapy. Cancer Med 2020. https://doi.org/10.1002/cam4.3634.

[21] Sannachi L, Gangeh M, Tadayyon H, Sadeghi-Naini A, Gandhi S, Wright FC, et al. Response monitoring of breast cancer patients receiving neoadjuvant chemotherapy using quantitative ultrasound, texture, and molecular features. PLoS ONE 2018. https://doi.org/10.1371/journal.pone.0189634.

[22] Sannachi L, Gangeh M, Naini A-S, Bhargava P, Jain A, Tran WT, Czarnota GJ. Quantitative ultrasound monitoring of breast tumour response to neoadjuvant chemotherapy: comparison of results among clinical scanners. Ultrasound Med Biol 2020;46(5):1142–57. https://doi.org/10.1016/j.ultrasmedbio.2020.01.022.

[23] Yao LX, Zagzebski JA, Madsen EL. Backscatter coefficient measurements using a reference phantom to extract depth-dependent instrumentation factors. Ultrason Imaging 1990;12(1):58–70. https://doi.org/10.1177/016173469001200105.

[24] Tadayyon H, Sadeghi-Naini A, Wirtzfeld L, Wright FC, Czarnota G. Quantitative ultrasound characterization of locally advanced breast cancer by estimation of its scatterer properties: ultrasonic breast cancer characterization. Med Phys 2014;41(1):012903. https://doi.org/10.1118/1.4852875.

[25] Haralick RM, Shanmugam K, Its'Hak D. Textural features for image classification. IEEE Trans Syst, Man Cybern 1973;SMC-3:610–21. https://doi.org/10.7497/j.issn.2095-3941.2013.02.007.

[26] Creff G, Devillers A, Depeursinge A, Palard-Novello X, Acosta O, Jegoux F, Castelli J. Evaluation of the prognostic value of FDG PET/CT parameters for patients with surgically treated head and neck cancer: a systematic review. JAMA Otolaryngol Head Neck Surg 2020;146(5):471. https://doi.org/10.1001/jamaoto.2020.0014.

[27] Leger S, Zwanenburg A, Pilz K, Zschaeck S, Zöphel K, Kotzerke Jörg, Schreiber A, Zips D, Krause M, Baumann M, Troost EGC, Richter C, Löck S. CT imaging during treatment improves radiomic models for patients with locally advanced head and neck cancer. Radiother Oncol 2019;130:10–7. https://doi.org/10.1016/j.radonc.2018.07.020.

[28] Robin P, Abgral R, Valette G, Le Roux P-Y, Keromnes N, Rousset J, Potard G, Palard X, Marianowski R, Salaun P-Y. Diagnostic performance of FDG PET/CT to detect subclinical HNSCC recurrence 6 months after the end of treatment. Eur J Nucl Med Mol Imaging 2015;42(1):72–8. https://doi.org/10.1007/s00259-014-2889-1.

[29] Diamant A, Chatterjee A, Vallières M, Shenouda G, Seuntjens J. Deep learning in head & neck cancer outcome prediction. Sci Rep 2019. https://doi.org/10.1038/s41598-019-39206-1.

[30] Jansen JFA. Texture analysis on parametric maps derived from dynamic contrast-enhanced magnetic resonance imaging in head and neck cancer. WJR 2016;8(1):90. https://doi.org/10.4329/wjr.v8.i1.90.